Title

The impact of alternative trait-scaling hypotheses for the maximum photosynthetic carboxylation rate (Vcmax) on global gross primary production

Journal

New Phytologist, 215(4)

ISSN

0028-646X

Authors

Walker, Anthony P

Quaife, Tristan

van Bodegom, Peter M

et al.

Publication Date

2017-09-01

DOI

10.1111/nph.14623

Peer reviewed

New Phytologist

The impact of alternative trait-scaling hypotheses for the maximum photosynthetic carboxylation rate (V_{cmax}) on global gross primary production

Anthony P. Walker[1,2], Tristan Quaife[3], Peter M. van Bodegom[4], Martin G. De Kauwe[5], Trevor F. Keenan[6], Joanna Joiner[7], Mark R. Lomas[2], Natasha MacBean[8], Chongang Xu[9], Xiaojuan Yang[1] and F. Ian Woodward[2]

[1]Oak Ridge National Laboratory, Environmental Sciences Division and Climate Change Science Institute, Oak Ridge, TN 37830-6301, USA; [2]Department of Animal and Plant Sciences, University of Sheffield, Alfred Denny Building, Western Bank, Sheffield, S10 2TN, UK; [3]Department of Meteorology, National Centre for Earth Observation, University of Reading, Reading, RG6 6BX, UK; [4]Institute of Environmental Sciences, Leiden University, 2333 CC, Leiden, the Netherlands; [5]Department of Biological Sciences, Macquarie University, Sydney, NSW 2109, Australia; [6]Earth Sciences Division, Lawrence Berkeley National Lab, 1 Cyclotron Road, Berkeley, CA 94720, USA; [7]NASA Goddard Space Flight Center, Greenbelt, MD 20771, USA; [8]Laboratoire des Sciences du Climat et de l'Environnement, LSCE/IPSL, CEA-CNRS-UVSQ, Université Paris-Saclay, Gif-sur-Yvette F-91191, France; [9]Earth and Environmental Sciences Division, Los Alamos National Laboratory, Los Alamos, NM 87544, USA

Author for correspondence:
Anthony P. Walker
Tel: +1 865 576 9365
Email: walkerap@ornl.gov

Received: *7 February 2017*
Accepted: *13 April 2017*

New Phytologist (2017) **215:** 1370–1386
doi: 10.1111/nph.14623

Key words: assumption-centred modelling, co-ordination hypothesis, Dynamic Global Vegetation Model (DGVM), gross primary production (GPP), modelling photosynthesis, plant functional traits, terrestrial carbon cycle, trait-based modelling.

Summary

- The maximum photosynthetic carboxylation rate (V_{cmax}) is an influential plant trait that has multiple scaling hypotheses, which is a source of uncertainty in predictive understanding of global gross primary production (GPP).
- Four trait-scaling hypotheses (plant functional type, nutrient limitation, environmental filtering, and plant plasticity) with nine specific implementations were used to predict global V_{cmax} distributions and their impact on global GPP in the Sheffield Dynamic Global Vegetation Model (SDGVM).
- Global GPP varied from 108.1 to 128.2 PgC yr^{-1}, 65% of the range of a recent model intercomparison of global GPP. The variation in GPP propagated through to a 27% coefficient of variation in net biome productivity (NBP). All hypotheses produced global GPP that was highly correlated (r = 0.85–0.91) with three proxies of global GPP.
- Plant functional type-based nutrient limitation, underpinned by a core SDGVM hypothesis that plant nitrogen (N) status is inversely related to increasing costs of N acquisition with increasing soil carbon, adequately reproduced global GPP distributions. Further improvement could be achieved with accurate representation of water sensitivity and agriculture in SDGVM. Mismatch between environmental filtering (the most data-driven hypothesis) and GPP suggested that greater effort is needed understand V_{cmax} variation in the field, particularly in northern latitudes.

Introduction

Photosynthetic carbon (C) assimilation is the largest flux in the global C cycle, and accurate future projections from terrestrial biosphere models (TBMs) rely upon accurate representations of photosynthesis. Rates of photosynthesis are most commonly simulated as the minimum carboxylation rate of two processes – the Calvin–Benson cycle and light-activated electron transport – modelled using Michaelis–Menten principles of enzyme kinetics (Farquhar *et al.*, 1980; Harley *et al.*, 1992; von Caemmerer, 2000). These two realized rates are sensitive to their respective maximum rates – the maximum carboxylation rate (V_{cmax}) and the maximum electron transport rate (J_{max}) – and terrestrial C cycle models are highly sensitive to these parameters (Zaehle *et al.*, 2005; Bonan *et al.*, 2011; Rogers, 2014; Sargsyan *et al.*, 2014; Rogers *et al.*, 2017). Many methods are used across TBMs to calculate V_{cmax} and J_{max}, and these methods represent competing hypotheses, formally or informally posed, about how these influential plant traits scale geographically. The diversity of hypotheses potentially leads to large, and previously unquantified, variation in the simulation of global photosynthetic C assimilation and poses the broader scientific question: what are the primary drivers of global V_{cmax} scaling?

Plant functional traits consist of a wide range of measurable plant phenotypic (chemical, physiological, and structural) properties that convey information pertaining to some aspect of plant function, and thus are used to describe plant function and functional diversity. Correlations between functional traits have been used to define common axes of plant strategies (Grime, 1974; Craine *et al.*, 2002; Wright *et al.*, 2004; Reich, 2014) and discrete plant functional types (PFTs), designed to simplify the diversity of plant life within a tractable modelling framework (Woodward

& Cramer, 1996; Smith *et al.*, 1998; Wullschleger *et al.*, 2014). The quantitative nature of plant functional traits makes them useful in global simulation modelling, allowing functions that represent the multiple ecosystem processes encoded in TBMs to be parameterized using values of the relevant plant functional traits. Recently, much attention has been paid to acknowledging wider and continuous variation in plant functional traits within ecosystem modelling (van Bodegom *et al.*, 2012, 2014; Pavlick *et al.*, 2013; Scheiter *et al.*, 2013; Verheijen *et al.*, 2013; Fyllas *et al.*, 2014; Fisher *et al.*, 2015; Kueppers *et al.*, 2016). Modelling this trait variation requires spatial and temporal trait-scaling hypotheses that go beyond the implicit hypothesis for many traits in many TBMs – that traits scale discretely across, and are static within, a limited set of broadly defined PFTs.

In the current study, multiple competing trait-scaling hypotheses for V_{cmax} and their impacts on global patterns of gross primary production (GPP) were assessed within a common modelling framework (the Sheffield Dynamic Global Vegetation Model (SDGVM)). Broadly defined, four V_{cmax} scaling hypotheses were investigated: (1) discrete PFT variation, (2) nutrient limitation, (3) environmental filtering, and (4) plant plasticity allowing acclimation to environment. As described above, discrete PFT variation is an hypothesis designed to represent key features of global diversity in plant function within a tractable modelling framework.

In more detail, nutrient, specifically nitrogen (N), limitation is hypothesized to affect V_{cmax} as a result of the high concentrations of the enzyme Rubisco in leaves which makes up a large portion of whole-plant N demand. Empirically, V_{cmax} and photosynthetic rates correlate with leaf N (Field & Mooney, 1986; Wright *et al.*, 2004; Kattge *et al.*, 2009) and plant N uptake (Woodward & Smith, 1995). SDGVM incorporates the hypothesis that plant N status is based on the principle of costs associated with plant N uptake as soil C increases and across mycorrhizal types (Read, 1991; Woodward *et al.*, 1995). This hypothesis has been expanded on by recent model development efforts (Fisher *et al.*, 2010; Brzostek *et al.*, 2014). The environmental filtering hypothesis states that adaptation to local environment is the primary determinant of V_{cmax} scaling. In our study, a data-driven approach was taken to represent environmental filtering of V_{cmax} following Verheijen *et al.* (2013). Plant plasticity, which allows acclimation to environment, is based on the hypothesis that the process of natural selection has created plants able to respond to their environment at shorter timescales (e.g. days to weeks). These plant-centric methods tend to consider an optimality perspective whereby plants adjust V_{cmax} to maximize the difference between costs and benefits (Chen *et al.*, 1993; Maire *et al.*, 2012; Prentice *et al.*, 2014).

Our aims were to quantify and understand the causes of variability across these various scaling hypotheses of: (1) global V_{cmax} distributions; (2) simulated global distributions of GPP; and (3) temporal trends in global GPP and subsequent impacts on net biome productivity, the simulation of which is the primary purpose of global TBMs. To evaluate the spatial patterns of global GPP predicted by the various methods to scale V_{cmax} we used a number of global GPP observation proxies: the Max Planck Institute (MPI) upscaled eddy-flux estimate of GPP (Jung *et al.*, 2011); global solar-induced fluorescence (SIF) from the Global Ozone Monitoring Experiment – 2 (GOME-2) instrument (Joiner *et al.*, 2013, 2016), and the Carnegie Ames Stanford Approach (CASA) model calibrated using SIF data.

Description

The SDGVM was developed as a daily timestep, global biogeography and eco-physiology model (Woodward *et al.*, 1995; Woodward & Lomas, 2004) to predict the primary biomes of Earth and their associated fluxes of C and water in response to global change. SDGVM has been described and extensively evaluated at site and global scales (Woodward *et al.*, 1995; Cramer *et al.*, 2001; Woodward & Lomas, 2004; Picard *et al.*, 2005; Sitch *et al.*, 2008; Beer *et al.*, 2010; De Kauwe *et al.*, 2013, 2014; Friend *et al.*, 2014; Walker *et al.*, 2014b; Zaehle *et al.*, 2014), so here we provide a brief description of the model and the process simulation methods relevant to this paper.

In SDGVM, C and water cycles conserve mass, while canopy N is simulated through an empirical relationship of N uptake to soil C (Woodward *et al.*, 1995; Woodward & Lomas, 2004), based on the principle of costs associated with plant N uptake as soil C increases and across mycorrhizal types (Read, 1991). During the application of SDGVM to the Free Air CO_2 enrichment (FACE) experiment model data synthesis (FACE-MDS; Walker *et al.*, 2014b; Medlyn *et al.*, 2015) it was observed that SDGVM had low V_{cmax} values at a standard temperature of 25°C ($V_{cmax,25} = 11N_a$, where N_a is leaf N per unit leaf area) and that using realistic values of $V_{cmax,25}$ observed at the FACE sites led to overprediction of GPP. The default $V_{cmax,25}$ values in SDGVM were calibrated to compensate biases caused by the assumption that photosynthesis calculated at mean daily radiation can be scaled by daylength to calculate mean daily photosynthesis. This assumption overestimates photosynthetic efficiency by effectively linearizing the response of photosynthesis to light. We corrected this bias by developing a sub-daily downscaling of light and photosynthesis calculations to 10 time periods during a half day (described in more detail in Supporting Information Notes S1). The sub-daily calculation of photosynthesis allowed realistic $V_{cmax,25}$ values to generate realistic values of GPP in the model. SDGVM scales $V_{cmax,25}$ and $J_{max,25}$ by water limitation and leaf age.

In view of their strong correlation, in this study we focus only on V_{cmax} scaling hypotheses and employ a single relationship of $V_{cmax,25}$ to $J_{max,25}$ (Walker *et al.*, 2014a):

$$J_{max,25} = eV_{cmax,25}^{0.890}. \quad \text{Eqn 1}$$

Each V_{cmax} scaling hypothesis – PFT, nutrient limitation, environmental filtering, and plant plasticity – for V_{cmax} scaling described in the Introduction was implemented in the SDGVM in multiple ways using a number of data sets, empirical relationships, and specific mathematical representations (see detailed

Table 1 Summary of V_{cmax} and maximum photosynthetic carboxylation rate (V_{cmax}) temperature scaling hypotheses

Hypothesis	Label	Specific method	PFT specific	Description	Reference	Papers/models	Data set
Static	Static_PFT	Static	Y	Augmented TRY database means	Verheijen *et al.* (2015)	Most CMIP5 models	Literature search augmented TRY
Nutrient limitation	Ntemp_global	Empirical f(N_u)	N		Woodward *et al.* (1995)	Original SDGVM	Woodward *et al.* (1995)
	N_global	Empirical f(N_a)	N	Power law	Walker *et al.* (2014a,b)		Literature search Walker *et al.* (2014a)
	NP_global	Empirical f(N_a, P_a)	N	Power law including leaf phosphorus	Walker *et al.* (2014a,b)		Literature search Walker *et al.* (2014a)
	N_PFT	Empirical f(N_a)	Y	Linear from TRY database	Kattge *et al.* (2009)	O-CN, other N cycle models	TRY
	N_oxisolPFT	Empirical f(N_a)	Y	As above but with oxisol relationship for evergreen broadleaf PFT	Kattge *et al.* (2009)		TRY
Environmental filtering	Environ_PFT	Empirical f(env.)	Y	Augmented TRY relationship to . . .	Verheijen *et al.* (2015)		Literature search augmented TRY
Plant plasticity	Co-ord_global	Theoretical f(Q, T, VDP)	N	V_{cmax} adjusted so $w_c = w_j$ given mean environment over the past 30 d	Chen *et al.* (1993); Maire *et al.* (2012)	First principles Wang *et al.*	N_a
Plant plasticity and nutrient limitation	LUNA_global	4. Theoretical f(N_a, Q, T, RH)	N	Constrained optimization of leaf N allocation given mean environment over the past 30 d	Xu *et al.* (2012); Ali *et al.* (2016)	CLM5.0	Literature search Ali *et al.* (2015)
	Temperature scaling						
Static	*	SDGVM default	N	Saturating exponential		SDGVM	
Static	*_modA	Modified Arrhenius	Y	Temperature optimum	Medlyn *et al.* (2002)		
Plant plasticity	*_tacc	Modified Arrhenius with acclimation	Y (modA only)	Temperature optimum varies with growth temperature	Kattge & Knorr (2007)		

N, no; N_u, N uptake; N_a, N per unit leaf area; P_a, P per unit leaf area; PFT, plant functional type; Q, incident photosynthetically active radiation per unit leaf area; SDGVM, Sheffield Dynamic Global Vegetation Model; T, leaf temperature; VPD, vapour pressure deficit; RH, relative humidity; Y, yes.
*The label for one of four V_{cmax} scaling hypotheses (N_global, N_PFT, LUNA_global, or Co-ord_global) used in conjunction with these three temperature scaling hypotheses.

descriptions of the implementations in the Methods below and Table 1).

Static traits (Static_PFT)

Static values of $V_{cmax,25}$ were derived by taking PFT means (using SDGVM PFT definitions; see Notes S1 for specific values) from the TRY database (www.try-db.org; data accession on 16 November 2010) augmented to include data from the sparsely represented tropics (described in the 'Environmental filtering' section below). This augmented TRY database was also used to derive the trait–environment relationships and is described in the Environmental Filtering section below. Each trait observation was linked to a PFT based on information on growth form (shrub, grass or tree), leaf habit (deciduous or evergreen) and photosynthetic pathway (C_3 or C_4) (Verheijen *et al.*, 2013, 2015).

Nutrient limitation hypotheses

We employ five implemetations of the nutrient limitation hypothesis. First (Ntemp_global), the original version of SDGVM calculated V_{cmax} from the rate of N uptake (N_u) (Woodward & Smith, 1994, 1995). N_u was calculated as a function of soil C, N, and mean annual air temperature (for details, see Woodward *et al.*, 1995). We label the original SDGVM method according to the assumption that sets it apart from other nutrient limitation hypotheses, that N_u is a function of temperature.

In later versions of SDGVM, the temperature modifier of N_u was removed and canopy N was calculated using a globally uniform, empirical scalar on N_u (Woodward *et al.*, 1995; Woodward & Lomas, 2004). All of the remaining implementations of the nutrient limitation hypotheses use the temperature-independent function of N_u and canopy N. The second implementation of the nutrient limitation hypothesis (N_global) was:

$$V_{cmax,25} = e^{3.712} N_a^{0.650}, \quad \text{Eqn 2}$$

where N_a is leaf N, and was taken from Walker *et al.* (2014a) and implemented globally. Third (N_PFT), we used the PFT-specific, linear $V_{cmax,25}$ to N_a relationships derived by Kattge *et al.* (2009). Fourth (N_oxisolPFT), to simulate an implicit phosphorus (P) limitation, we used the N_PFT relationships but replaced the evergreen broadleaved PFT relationship with a relationship derived on P-poor oxisols. Fifth (NP_global), to simulate a more explicit P limitation on $V_{cmax,25}$, a function of $V_{cmax,25}$ where P was influential in interaction with N derived from a database of field- and laboratory-grown plants (Walker *et al.*, 2014a) was also simulated:

$$V_{cmax,25} = e^{3.946} N_a^{[0.921+0.282\ln(P_a)]} P_a^{0.121}. \quad \text{Eqn 3}$$

To simulate leaf P concentration, we used a global relationship to total soil P derived by Ordonez *et al.* (2009), and a global total soil P map (Yang *et al.*, 2014).

Environmental filtering

Environmental filtering was represented by empirically deriving PFT-specific trait–environment relationships (Environ_PFT) from the TRY database $V_{cmax,25}$ values at the accession date (Niinemets, 1999; Kattge *et al.*, 2009) augmented by Verheijen *et al.* (2015) to include $V_{cmax,25}$ from the tropics (Deng *et al.*, 2004; Meir *et al.*, 2007; Domingues *et al.*, 2010; Cernusak *et al.*, 2011; van de Weg *et al.*, 2011; Azevedo & Marenco, 2012; Nascimento & Marenco, 2013) which were not well covered in the TRY database. Each species within the database was assigned to a PFT based on the specific SDGVM PFT definitions.

Based on the global coordinates of the trait data, each trait entry was associated with a set of environmental conditions – mean annual temperature, mean temperature of the warmest month, mean temperature of the coldest month, temperature difference of the warmest month and coldest month, total annual precipitation, total precipitation in the driest quarter, fraction of total precipitation that falls in the driest quarter, mean annual relative humidity, and total annual down-welling shortwave radiation – taken from the Climatic Research Unit and National Centers for Environmental Prediction (CRUNCEP) data set (the same as used to run the model simulations). For each PFT, a multiple regression with forward selection was run to relate variation in $V_{cmax,25}$ to environmental drivers. To avoid correlation between explanatory variables, variables with a correlation > 0.7 were not used in the same regression model.

An empirical, linear decrease in $V_{cmax,25}$ with CO_2 calculated using the formulation of Verheijen *et al.* (2015) was also included as part of the response to environment (see Notes S1 for the relationships). $V_{cmax,25}$ is calculated at the beginning of each year for each PFT on each grid square based on the mean environmental conditions of the past year.

V_{cmax} data for C_4 plants were only available for these trait–environment relationships. Therefore, in the simulations for all hypotheses, these relationships (or static values for Static_PFT) were used to set $V_{cmax,25}$ and phosphoenolpyruvate carboxylase ($PepC_{25}$) activity in C_4 plants.

Plant plasticity

We examined plant plasticity by using the co-ordination hypothesis (Co-ord_global), which states that plants adjust V_{cmax} such that the carboxylation-limited rate of photosynthesis (w_c) equals the electron transport-limited rate of photosynthesis (w_j) over mean environmental conditions, commonly considered those of the past month (Chen *et al.*, 1993; Maire *et al.*, 2012). Using the Harley *et al.* (1992) photosynthesis functions, the co-ordination hypothesis to find V_{cmax} requires solving the following function (see Notes S1 for derivation):

$$0 = V_{cmax}(4C_i + 8\Gamma_*) \left[1 + \left(\frac{\alpha_i \overline{Q}}{S_{t,j} e (V_{cmax}/S_{t,v})^{0.890}}\right)^2\right]^{0.5} - \alpha_i \overline{Q}(C_i + K_m) \quad \text{Eqn 4}$$

(C_i, the internal CO_2 partial pressure (Pa); Γ_*, the photorespiratory CO_2 compensation point (Pa); α_i, the intrinsic quantum efficiency of electron transport (mol mol^{-1} absorbed photons); $\overline{Q}$, the mean absorbed light intensity of the past month (μmol m^{-2} s^{-1}); $S_{t,j}$ and $S_{t,v}$, the temperature scalars for $J_{max,25}$ and $V_{cmax,25}$ to scale to leaf temperature from 25°C; e, the base of the natural logarithm; K_m, the effective Michaelis–Menten half-saturation constant for carboxylation when accounting for oxygenation (Pa).) The denominator in the squared term, $S_{t,j} e (V_{cmax}/S_{t,v})^{0.890}$, represents J_{max} at the mean temperature of the last month calculated using Eqn 1 and considering temperature scaling.

The leaf N utilization for assimilation (LUNA) (Xu *et al.*, 2012; Ali *et al.*, 2016) hypothesis was also evaluated (LUNA_global). LUNA optimizes leaf N investment in various photosynthetic functions – light capture, electron transport and carboxylation – to maximize daily net photosynthesis (assimilation − leaf respiration) given mean environmental conditions (Ali *et al.*, 2016). The LUNA optimization also satisfies empirical environmental constraints and the constraint of co-ordination of w_c and w_j. Thus, LUNA is a combination of plant plasticity, nutrient limitation, and environmental filtering hypotheses.

In this study we use the mean environmental conditions of the past 30 d, consistent with the averaging used for the co-ordination hypothesis (Ali *et al.*, 2016 use the previous 10 d).

Scaling of $V_{cmax,25}$ to leaf temperature

Being enzymatically controlled, at short timescales V_{cmax} is highly dependent on leaf temperature and is usually normalized to a reference temperature, commonly 25°C, adding the subscript 25 to the notation ($V_{cmax,25}$). Three methods used to

scale $V_{cmax,25}$ to leaf temperature were investigated (see Fig. S1 and Notes S1 for more details): (1) a saturating exponential (the SDGVM model default); (2) the Arrhenius equation modified for enzymatic loss of function at high temperatures as presented in Medlyn *et al.* (2002); and (3) the modified Arrhenius with emprical acclimation of temperature optima to local environmental conditions (Kattge & Knorr, 2007).

Model set-up and simulations

The model simulations were run using the CRUNCEP meteorological data set 1901–2012 (Le Quéré *et al.*, 2014; Figs S2–S4). PFT distributions were assumed to be static throughout the whole simulation period and were derived from land cover (LC) maps provided by the European Space Agency Climate Change Initiative (www.esa-landcover-cci.org; Figs S5–S12). The PFT fractions were derived from the LC maps using the LC to PFT conversion described in Poulter *et al.* (2015), and adjusted to account for the separation of C_3 and C_4 species that cannot be detected using medium resolution imaging spectrometer wavebands (Poulter *et al.*, 2015). The resultant PFT maps were then further categorized according to the SDGVM PFT classification.

Atmospheric CO_2 data were taken from the Scripps Ocean Institute merged ice-core and flask measurement global data set (Keeling *et al.*, 2005). The simulations were initialized with a 500-yr spin-up that randomly selected meteorological years from the period 1901–1920. A separate spin-up was conducted for each ensemble member. The ensemble consisted of the nine different trait-based approaches to simulate V_{cmax} (Table 1) and a subset of these nine approaches – N_global, N_PFT, Co-ord_global, and LUNA_global – each run with the three temperature scaling assumptions, for a total of 17 simulations. N_-global, N_PFT, Co-ord_global, and LUNA_global were chosen to combine with the three temperature scaling approaches to represent a range of methods, and to see how the temperature scaling assumptions interacted with the dynamic spatial-scaling plant plasticity hypotheses (i.e. Co-ord_global and LUNA_global).

Evaluation data sets

The simulated spatial distributions of global GPP were used to evaluate the impacts of the various V_{cmax} simulation methods. No method exists to measure GPP directly at the global scale; all methods involve assumptions and models (Anav *et al.*, 2015) that may introduce bias or nonindependence from the SDGVM simulations. We therefore compared modelled spatial distributions of GPP to three global GPP proxies – the empirically up-scaled flux tower estimates of GPP from the MPI (Beer *et al.*, 2010; Jung *et al.*, 2011), and two data sets based on GOME-2 SIF (Joiner *et al.*, 2013, 2016).

The two SIF-based methods differed in their scaling of SIF radiance ($Wm^{-2}\,sr^{-1}\,yr^{-1}$) to GPP ($gC\,m^{-2}\,yr^{-1}$). The first scaling method (SIF-CASA) scaled SIF using modelled GPP from the CASA Global Fire Emissions Database version 3 (GFED 3) model (van der Werf *et al.*, 2010). CASA primarily determined the spatial variation in GPP while SIF determined the temporal variation: in each gridpoint, monthly SIF data were normalized by the gridpoint mean and then multiplied by the gridpoint mean CASA-GFED GPP (Eqn 5; SIF-CASA). The second scaling method (scaled-SIF) was intended to allow SIF to determine both temporal and spatial variation in GPP: SIF values were annually integrated in each grid cell, normalized by the global mean SIF ($\bar{SIF}$) and then multiplied by the global mean of the SIF-CASA data set (Eqn 6).

$$cSIF_{i,j,t} = \frac{\bar{CASA}_{i,j}.SIF_{i,j,t}}{\bar{SIF}_{i,j}}, \quad \text{Eqn 5}$$

$$s\bar{S}IF_{i,j} = \frac{cSIF.\bar{SIF}_{i,j}}{\bar{SIF}} \quad \text{Eqn 6}$$

($\bar{CASA}$, the CASA GPP; cSIF, the CASA scaled GPP; sSIF, the simply scaled SIF; subscripts are the gridpoint latitude, *i*; longitude, *j*; and time, *t*.)

At the time of writing, SIF data were available for the period 2007–2012 and so for consistency we present analyses for all model output over the same period. A comparison of model results for the last full decade, 2001–2010, with 2007–2012 gave quantitatively similar results. The MPI data were available only until 2011, but given that the MPI data have little inter-annual variability (Kumar *et al.*, 2016) this was expected to have little effect.

GPP values predicted by the trait-scaling hypotheses were compared against the three GPP proxies using standard deviation (SD), correlation, and centred root mean square difference. Combining these metrics in polar co-ordinates allows comparison of gridded data sets against a reference. These plots are known as Taylor diagrams (Taylor, 2001). Data sets were also analysed using principal component analysis (PCA) to identify common axes of variation across the data sets. As well as hypotheses and GPP proxies, climate variables (temperature, precipitation, and short-wave radiation (SWR)) were included to investigate climatic influence in the spatial patterns. Data sets were mean centred and scaled by SD to give *z*-scores before conducting the PCA. The R (R Core Development Team, 2011) package PLOTRIX (Lemon, 2006) was used to plot the Taylor diagrams and the function PRCOMP from the STATS package to perform the PCA.

Results

Global $V_{cmax,25}$ distributions

Global distributions of top-leaf $V_{cmax,25}$ predicted by the various trait scaling assumptions had markedly different means, variances, and latitudinal distributions (Figs 1, S13). All but one (Ntemp_global) nutrient limitation hypothesis including LUNA_global (which is constrained by nutrient limitation) predicted relatively low variance in global $V_{cmax,25}$, with moderate values in the tropics, high values in the temperate zone, the highest values in dry temperate regions, and the lowest values in the

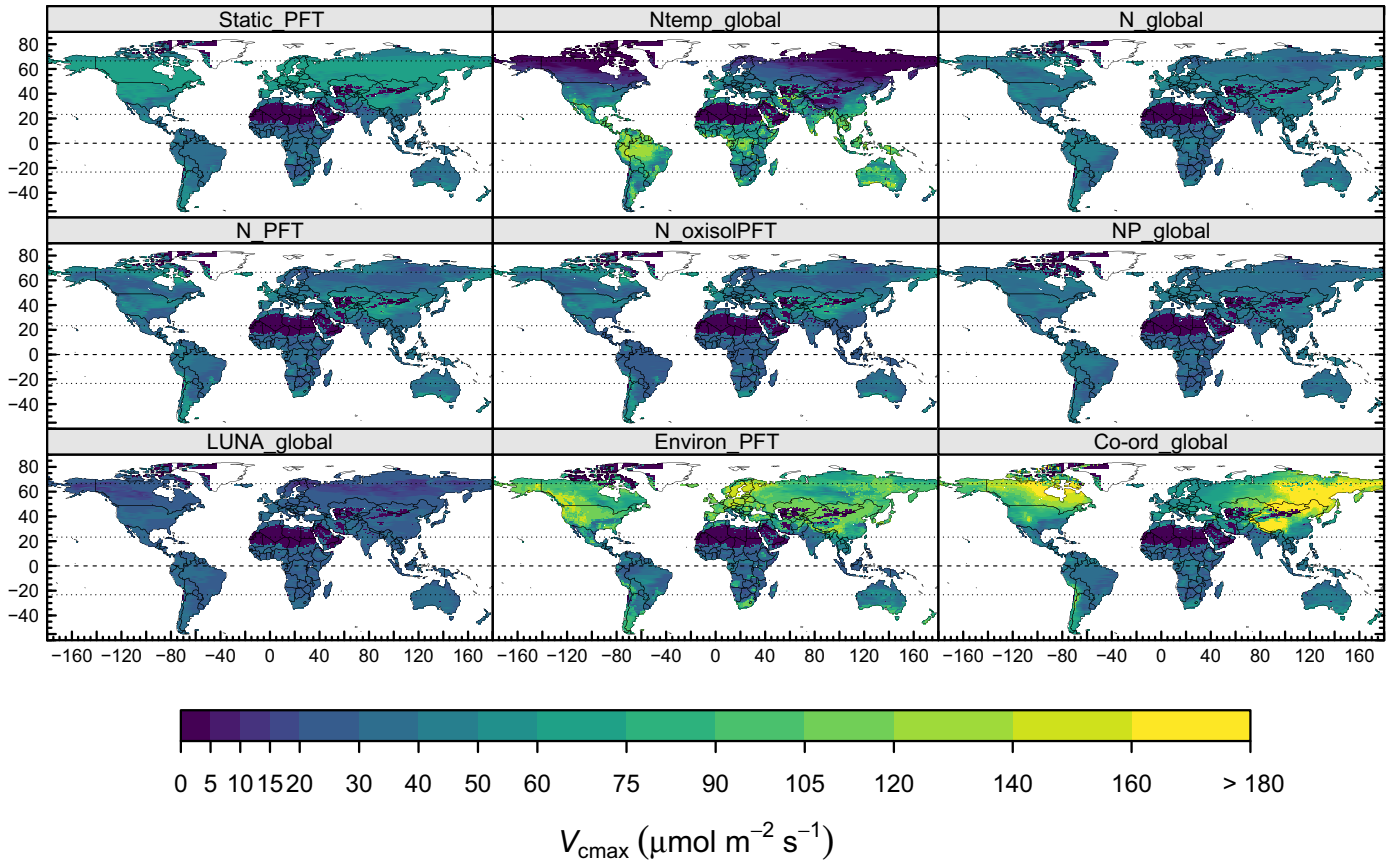

Fig. 1 Mean growing season top-leaf maximum photosynthetic carboxylation rate at 25°C $V_{cmax,25}$ (μmol m^{-2} s^{-1}) over the period 2007–2012 for the nine implementations of the four V_{cmax} trait-scaling hypotheses. Growing season is defined as a period during which the leaf area index (LAI) was > 1. Values are reported before scaling of V_{cmax} by water stress or leaf age.

boreal zone before increasing in the high Arctic (Fig. 1). The exception (Ntemp_global) showed relatively high $V_{cmax,25}$ variance, with the highest values in the tropics which broadly decreased with latitude. Inclusion of P, either implicitly (N_oxisolPFT; Kattge *et al.*, 2009) for the evergreen broadleaf PFT in the simulation or explicitly (NP_global; Walker *et al.*, 2014a), reduced $V_{cmax,25}$ marginally in much of the tropics (compared with N_PFT and N_global, respectively).

By contrast, non-nutrient-based hypotheses (Static_PFT, Environ_PFT, and Co-ord_global) tended to show the opposite pattern (Figs 1, S13): more pronounced maximum $V_{cmax,25}$ values in northern cool wet areas dominated by green needle-leaf PFTs (Scandinavia and the North American Pacific coast) and dry areas dominated by C_3 grasses (the North American west and Central Asia). The Static_PFT values and the Environ_PFT relationships were derived from the same $V_{cmax,25}$ data set. Therefore, the observed similar latitudinal pattern was expected, as was the more spatially homogenous distribution for the static values per PFT. The co-ordination hypothesis is independent of the data sets used to produce the Static_PFT and Environ_PFT, and produced the highest $V_{cmax,25}$ values in the coldest and driest regions – north-eastern Canada and Asia, and the Himalayan plateau.

Consequences for the simulated carbon cycle

Across the nine $V_{cmax,25}$ scaling implementations, global mean annual GPP for the period 2007–2012 ranged from 108.1 to 128.2 PgC yr^{-1} (Fig. 2; Table 2). The ensemble mean ± SD annual GPP was 118.7 ± 6.4 PgC yr^{-1}, giving a coefficient of variation of 5.4% (Table 2). The variation was somewhat higher for vegetation and soil C stocks (12.0% and 13.9%, respectively). Most crucial for C sequestration from the atmosphere under global change was that net biome productivity (NBP) varied by 27.1% across the hypotheses tested.

The highest global GPP was simulated by the Ntemp_global implementation of nutrient limitation, closely followed by the static PFT hypothesis at 127.8 PgC yr^{-1}. The global and PFT specific relationships of $V_{cmax,25}$ to leaf N simulated global GPP of 121.7 and 116.5 PgC yr^{-1}. The inclusion of P as an additional limiting factor resulted in lower global GPP by 3.7 and 5.9 PgC yr^{-1}, respectively, than consideration of N limitation alone. The P-related drop in GPP was a result of disproportionate GPP reduction by P in generally high productivity regions, that is, the tropics (Figs 2, S14). Environmental filtering (Environ_PFT) and plant plasticity (Co-ord_global) simulated similar mean GPP at 118.1 and 119.2 PgC yr^{-1}. The constrained

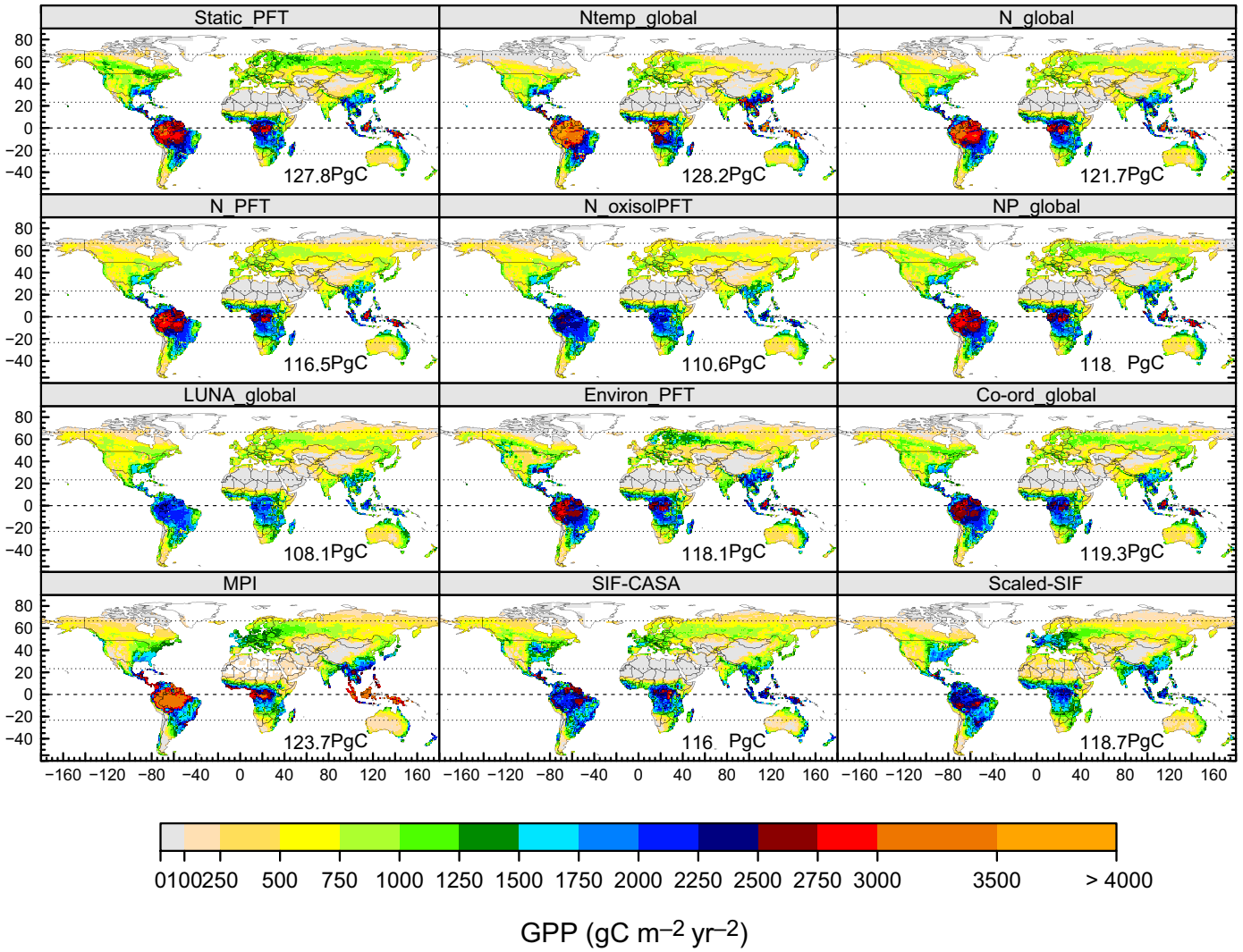

Fig. 2 Mean annual gross primary production (GPP) (gC m^{-2} yr^{-1}) for the period 2007–2012 for the nine implementations of the four maximum photosynthetic carboxylation rate (V_{cmax}) trait-scaling hypotheses and the three global GPP proxies. Global mean annual GPP is shown in each panel (PgC).

optimization of functional leaf N allocation (LUNA hypothesis) yielded the lowest GPP at 108.1 PgC yr^{-1}.

For a subset of $V_{cmax,25}$ scaling hypotheses (N_global, LUNA_global, and Co-ord_global), the more up-to-date modified Arrhenius temperature scaling (Medlyn *et al.*, 2002; Kattge & Knorr, 2007) was used, both with and without acclimation of temperature optima to growth temperature. Using these temperature scaling functions generally increased global GPP (Fig. S15), especially for the co-ordination hypothesis (119.1–131.2 PgC yr^{-1}). The increase in GPP for was primarily attributable to increasing GPP in the northern temperate and boreal zones (Fig. 3).

The hypotheses and their implementations also influenced the temporal trend in GPP (1900–2012) in response to increasing CO_2 and changing climate (Fig. 4a). Ntemp_global resulted in the strongest change in GPP over the 20th Century, the result of increasing temperatures stimulating N uptake. The LUNA hypothesis and the co-ordination hypothesis both predict shallower trajectories in GPP than any of the other scaling hypotheses. Scaling $V_{cmax,25}$ and $J_{max,25}$ using the modified Arrhenius function with and without temperature acclimation made little difference to the relative trajectories of GPP when used in conjunction with N_global, co-ordination, and LUNA hypotheses (Fig. S16). Across the ensemble, NBP over the period 2007–2012 was strongly related to the change in global GPP over the time period 1901–2012 (Fig. 4b).

Evaluating spatial distributions of GPP

Overlying the general, climatically driven spatial distribution of GPP, the differences in the spatial distributions of $V_{cmax,25}$ are observable in the simulated GPP distributions (Figs 2, S3). To evaluate the various hypotheses, their global GPP predictions (mean annual GPP over 2007–2012) are compared in Taylor space (Fig. 5; Table S1) with several GPP proxies (MPI, scaled-SIF, and SIF-CASA; Figs 2, S17). No matter which GPP proxy was taken as reference, all hypotheses clustered closely in Taylor space with a correlation of approximately $r = 0.9$ ($r = 0.85$–0.91),

Table 2 Carbon cycle variables for the nine maximum photosynthetic carboxylation rate (V_{cmax}) scaling hypotheses (means over the period 2007–2012)

	GPP	NPP	NBP	Csoil	Cveg	Ctotal
Static_PFT	127.8	73.4	1.7	1619.8	777.7	2397.5
Ntemp_global	128.2	71.1	2.9	1009.5	768.0	1777.5
N_global	121.7	66.8	2.1	1304.6	680.9	1985.5
N_PFT	116.5	64.9	1.9	1285.6	581.8	1867.4
N_oxisolPFT	110.6	62.5	1.6	1270.9	517.4	1788.3
NP_global	118.0	64.1	1.9	1289.6	694.2	1983.8
LUNA_global	108.1	60.9	1.2	1349.2	558.4	1907.7
Environ_PFT	118.1	66.2	1.9	1253.1	781.2	2034.3
Co-ord_global	119.3	69.6	1.1	1494.9	714.3	2209.2
Mean	118.7	66.6	1.8	1319.7	674.9	1994.6
SD	6.4	3.9	0.5	158.8	94.0	189.6
CV (%)	5.4	5.8	27.3	12.0	13.9	9.5

GPP, gross primary production; NBP, net biome productivity; NPP, net primary productivity; Csoil, soil carbon stocks; Cveg, vegetation carbon stocks; Ctotal, total terrestrial carbon stocks; SD, standard deviation; CV, coefficient of variation. All variables are in gC m^{-2} yr^{-1}.

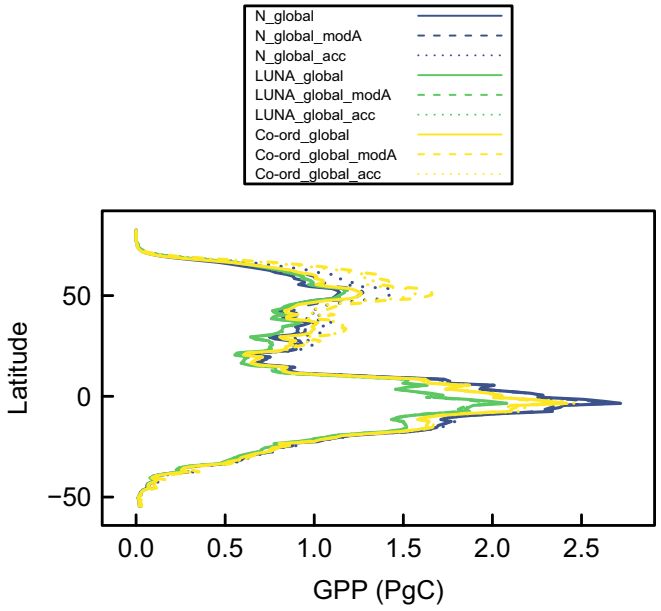

Fig. 3 Mean annual zonal gross primary production (GPP) (PgC) over the period 2007–2012 for three of the maximum photosynthetic carboxylation rate (V_{cmax}) trait-scaling implementations in combination with the three temperature scaling assumptions.

SD within ± 25% (with the exception of Ntemp_global compared against both SIF-based proxies and LUNA compared against MPI), and centred root mean square difference between 250 and 500 gC m^{-2} yr^{-1}. All hypotheses were marginally less correlated to the scaled-SIF data (r = 0.85–0.89) than the other two GPP proxies.

The hypotheses most closely correlated to MPI and SIF-CASA were N_global and N_PFT, although the improvements in the correlations were marginal (r = 0.91 vs 0.88–0.90). Ntemp_global was generally less well correlated to all three proxies with substantially higher SD and predicting the highest global GPP and strongest latitudinal gradient. The hypotheses that were least well correlated to MPI were LUNA_global and Environ_PFT, although again only marginally. Environ_PFT was also less well correlated with both SIF-based proxies. N_PFT and N_oxisolPFT were the most closely correlated to scaled-SIF, being marginally better than LUNA and N_global. The variance in the correlation across the hypotheses was greater when hypotheses were compared against the scaled-SIF proxy (Fig. 5c).

Difference plots between modelled GPP and GPP proxies (Figs 6, S18, S19) showed that the N_oxisolPFT implementation tended to perform well against all three proxies, although there were some substantial under-predictions in tropical forests when compared against MPI (Fig. S18). However, tropical GPP was consistently under-predicted by many implementations when compared against MPI, particularly in the Amazon. Static values per PFT and Ntemp_global clearly showed the strongest mismatches with the GPP proxies. Environ_PFT performed poorly in northern latitudes, particularly Scandinavia, and southern China, where V_{cmax} was predicted to be higher than any other implementation (Fig. 1). Co-ordination and LUNA performed well, but tended to over-predict in nothern latitudes when compared against N_PFT and N_oxisolPFT. Across all implementations, GPP was under-predicted in Europe, eastern North America, and India while GPP was over-predicted in grasslands, particularly in South America, western North America and sub-Saharan Africa.

When the alternative, more realistic modified Arrhenius temperature response hypotheses were implemented, mismatches with scaled-SIF were unaffected for LUNA_global, slightly worsened in N_global and N_PFT, and noticeably worsened for Co-ord_global (Fig. 5d). Implemented within the LUNA model, the three different temperature scaling assumptions made little difference to global GPP, presumably because the N constraint in LUNA was strong and the optimization allowed flexibility around temperature responses to find a similar maximum assimilation rate across temperature scaling assumptions.

The SIF-CASA, scaled-SIF and MPI proxies were generally more correlated to each other than to any of the V_{cmax} hypothesis implementations, but only marginally. Arguably, the proxies were as dissimilar from each other as the better model hypotheses were from the proxies, making it difficult to provide a definitive conclusion about which specific implementation of the various hypotheses was closest to GPP observation proxies.

Principal component (PC) analysis (PCA) was used to identify the common patterns and areas of divergence across both the models and the GPP proxies, and the potential climatic drivers of the commonalities and differences. PCA demonstrated that 82% of the spatial variance across simulated GPP, GPP proxies, and climatic variables was explained by a single PC (Fig. S20). All model assumptions were closely grouped with high loadings on PC1 (Fig. 7a); that is, all model predictions were positively correlated with the spatial pattern of the first PC (Fig. 7c). Closely grouped to the models on PC1 were all observed GPP proxies, as well as precipitation. SWR and temperature were less strongly correlated with PC1, although the correlation was also positive,

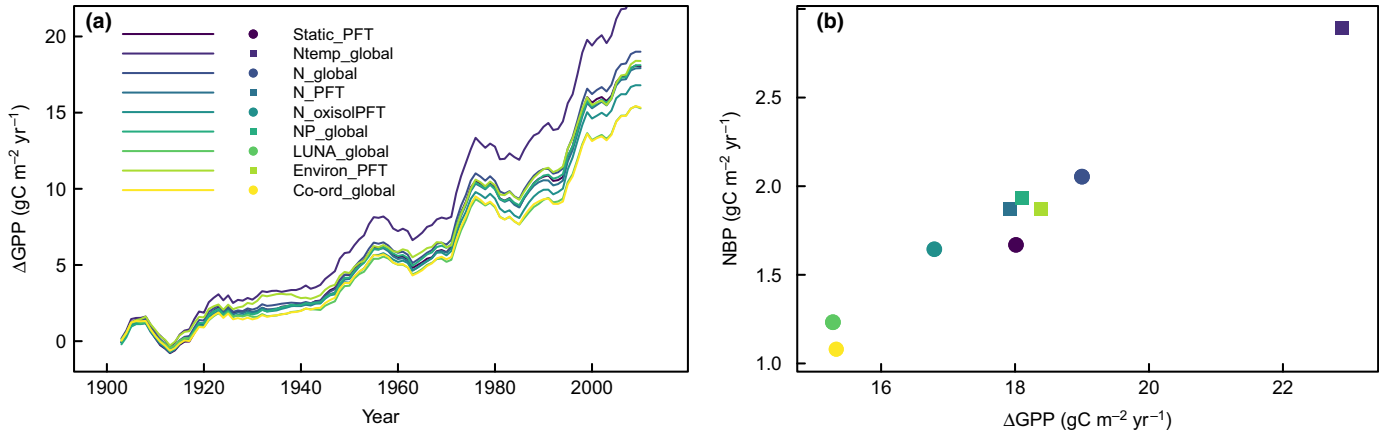

Fig. 4 Variability in gross primary production (GPP) trends and net biome productivity (NBP) for the nine implementations of the four maximum photosynthetic carboxylation rate (V_{cmax}) trait-scaling hypotheses. (a) Trends in the absolute change in global GPP over the period 1901–2012; and (b) the relationship between mean annual net biome productivity (NBP) for 2007–2012 and the change in GPP for 1901–2012 across the nine hypotheses. PFT, plant functional type.

suggesting that precipitation is the primary driver of the dominant global pattern in GPP.

PC2 accounted for *c.* 11% of spatial variance and segregated SWR and temperature (both positively correlated to PC2) from the model implementations, GPP proxies, and precipitation (Fig. 7d). The remaining PCs combined accounted for 7% of the spatial variation in the data and it was these remaining PCs that demonstrated the main areas of divergence between V_{cmax} implementations and GPP proxies.

PC3 and PC4 accounted for 4% of variation. SWR and modelled GPP were correlated with PC3, while the GPP proxies (MPI most strongly) and precipitation were anti-correlated. PC3 shows the regions where modelled GPP was stimulated by light (primarily in natural grasslands; blue areas Fig. 7e) or restricted by low light (red areas). By contrast, the GPP proxies appeared to be stimulated by precipitation (red areas) or restricted by low precipitation (blue areas). PC4 segregated both SIF proxies from precipitation. PC4 showed high values almost exclusively in the world's major agricultural regions – the North American cornbelt, the northeastern and southern regions of Brazil and the area surrounding São Paulo, Europe, the Russian bread basket, India, particularly northern India, central eastern China, and even smaller agricultural regions such as the Indus valley in Pakistan and alongside the Rift Valley in East Africa.

Discussion

We tested a series of plausible trait-scaling hypotheses for V_{cmax}, many of which are implemented in terrestrial ecosystem models, and found that they led to substantial variability in SDGVM simulated global GPP. Mean annual GPP ranged across the implementations of the hypotheses from 108.1 to 128.2 PgC yr^{-1} (mean ± SD 118.7 ± 6.4 PgC yr^{-1}). The range in global GPP demonstrates the high sensitivity of simulated GPP to V_{cmax} and this range encompasses 65% of that from a set of three models run in coupled and uncoupled modes (1990–2009 mean annual GPP range of 130–161 PgC yr^{-1}; mean ± SD 145.6 ± 12.6 PgC yr^{-1}; Anav *et al.*, 2015). The simulations used by Anav *et al.* (2015) were drawn from two inter-comparison projects, each with their own protocols, which is likely to inflate the range of simulated GPP compared with the simulations presented in this study, which share a single protocol. Thus, variation in simulated GPP caused by V_{cmax} trait scaling hypotheses probably represents a substantial source of variation in GPP across models, which is currently unaccounted for in model intercomparisons.

Dynamic trait-scaling based on nutrient limitation, in which plant nutrient status is inversely related to the cost of N acquisition, performed better than other hypotheses when compared against three GPP observation proxies. PFT specific relationships of V_{cmax} to leaf N resulted in the best performance. Static trait values per PFT were not supported by this study. The better performance of nutrient limitation implementations was most apparent when compared against the scaled-SIF GPP proxy and we argue that this is a more independent, and thus more robust, comparison.

Evaluation of V_{cmax} distributions

Discerning which is the most realistic trait-scaling hypotheses was nontrivial. Currently no independent, globally gridded estimates of $V_{cmax,25}$ distributions exist. Many regions in global V_{cmax} data sets are only sparsely represented and one of the most comprehensive global V_{cmax} data sets was employed to compile the $V_{cmax,25}$ relationships to environment (Environ_PFT) for the trait-filtering hypothesis (Kattge *et al.*, 2011; Verheijen *et al.*, 2013). The Environ_PFT prediction of the global $V_{cmax,25}$ distribution (Fig. 1) is an empirical upscaling of $V_{cmax,25}$ point measurements using global climatic and land-cover information. Unlike other hypotheses tested, which additionally rely on either model process representation (e.g. simulation of leaf N) or more theoretical assumptions (e.g. co-ordination), Environ_PFT is data-driven and contingent only on the assumption that $V_{cmax,25}$ scales with environment (coefficient of determination 0.49–0.82

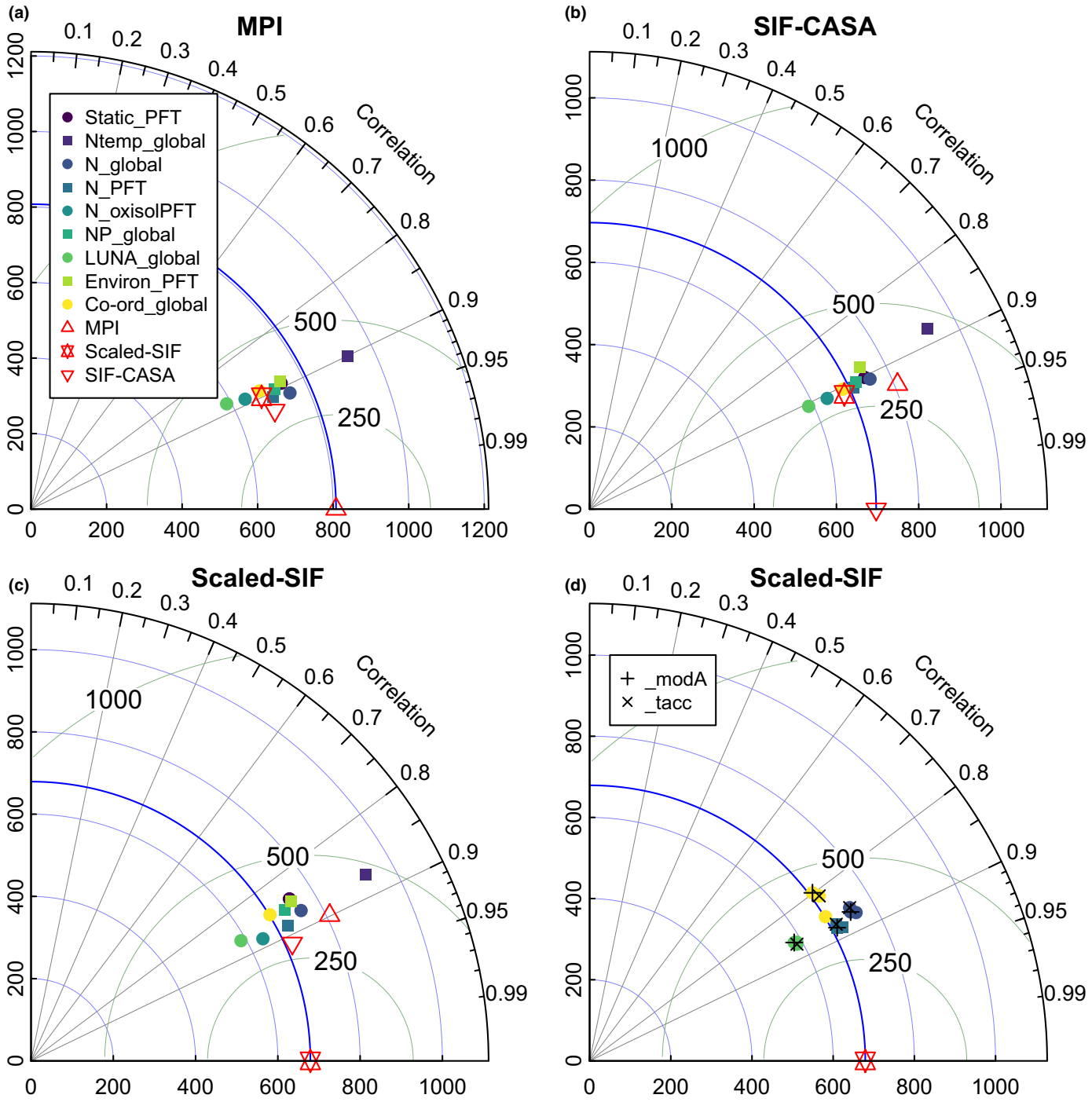

Fig. 5 Taylor plots of gross primary production (GPP) (2007–2012) for the nine implementations of the four maximum photosynthetic carboxylation rate (V_{cmax}) trait-scaling hypotheses compared against the three GPP proxies: (a) Max Planck Institute (MPI), (b) solar-induced fluorescence (SIF)-Carnegie Ames Stanford Approach (CASA), (c) scaled-SIF; and (d) including the two additional temperature scaling hypotheses (modA and tacc) for N_global, N_PFT, LUNA_global and Co-ord_global. Taylor plots compare data sets against a reference data set using correlation (grey radial isolines), standard deviation (blue circular isolines; zero at the origin), and root mean difference (green circular isolines; zero at the reference data set on the x-axis). PFT, plant functional type.

for C_3 plants; see Notes S1; and Ali *et al.*, 2015; Verheijen *et al.*, 2013).

The data-driven Environ_PFT $V_{cmax,25}$ values are higher in northern latitudes relative to the tropics, as are $V_{cmax,25}$ distributions for the co-ordination hypothesis, which is in line with current literature (A. Rogers *et al.*, unpublished). All the N-based hypotheses in SDGVM (including LUNA) generally showed higher $V_{cmax,25}$ in the tropics than in the boreal and

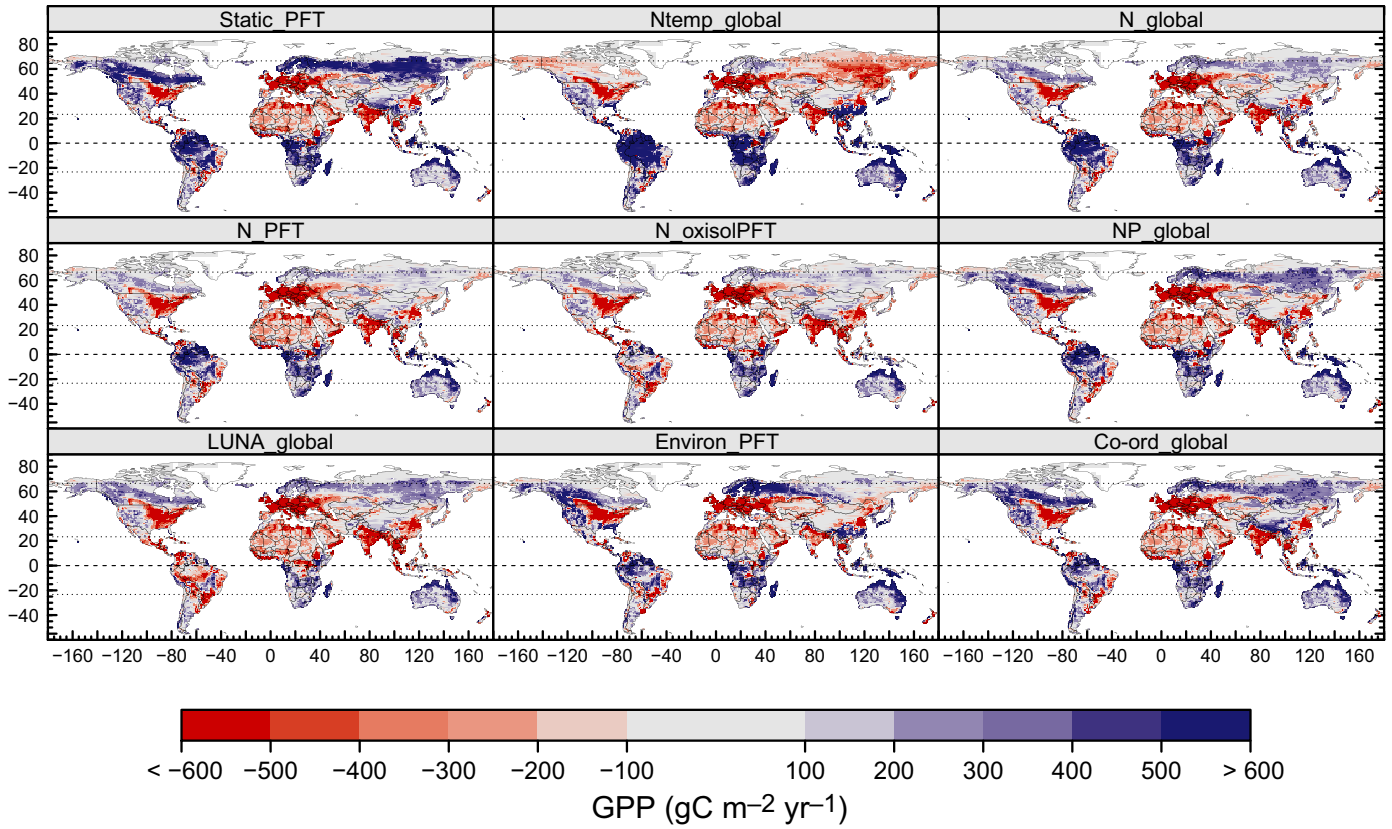

Fig. 6 Difference plot of gross primary production (GPP) simulated by the nine implementations of the four maximum photosynthetic carboxylation rate (V_{cmax}) trait-scaling hypotheses minus the scaled-solar-induced fluorescence (SIF) GPP proxy. PFT, plant functional type.

tundra zones (Fig. 1), which is not consistent with our data-driven estimate (Environ_PFT). N limitation hypothesis predictions of tropical $V_{cmax,25}$ were consistent with the literature, often reported in the range 20–80 μmol m^{-2} s^{-1} (Domingues *et al.*, 2010, 2015; Vårhammar *et al.*, 2015; Norby *et al.*, 2017), but were not consistent with values reported for the high Arctic, in the range 60–160 μmol m^{-2} s^{-1} (A. Rogers *et al.*, unpublished).

The primary cause of the zonal $V_{cmax,25}$ distribution for the implementations constrained by N is the core SDGVM hypothesis that plant nutrient status is inversely related to soil C. This hypothesis is based on observations that plant N uptake decreases as dependence on organic N supply (correlated with mycorrhizal N supply) increases, which in turn is hypothesized to be a consequence of increasing soil organic matter (Read, 1991; Woodward *et al.*, 1995). The global distributions of $V_{cmax,25}$ predicted by the nutrient limitation hypothesis are therefore generally the inverse of the distributions of soil C (Figs S21–S23), resulting in a broad latitudinal gradient in leaf N as soil decomposition rates slow with cooling temperatures. This cost-based hypothesis for plant N status reproduces the broad macro-ecological pattern of increasing N limitation as latitude increases suggested by leaf C : N and N : P stoichiometry (McGroddy *et al.*, 2004; Reich & Oleksyn, 2004; Ordonez *et al.*, 2009).

The original LUNA study at the global scale showed lower $V_{cmax,25}$ in the tropics and global distributions of top-leaf $V_{cmax,25}$ that were more similar to those predicted by Environ_PFT and Co-ord_global (Ali *et al.*, 2016) than the N limitation hypotheses to which LUNA was more similar in this study. The defining difference is that Ali *et al.* (2016) assumed a constant top-leaf N of 2 gm^{-2}, while in SDGVM leaf N varies as a function of soil C. The results in SDGVM suggest that LUNA is more sensitive to variability in leaf N than to variability in environment.

Evaluation of GPP distributions

PCA demonstrated that precipitation was the primary driver of the dominant mode of global GPP distributions in both the GPP proxies and all model simulations, and was therefore responsible for the strong correlation (0.85–0.91) of all hypotheses to the proxies. PCA indicated that the model simulations diverged from the observation proxies for two reasons: (1) a relative GPP stimulation by photosynthetically active radiation (PAR) in dry grasslands in SDGVM opposing a relative GPP reduction by low precipitation in the proxies (and vice versa; PC3); and (2) a relative stimulation of GPP in SIF-based proxies in agricultural areas of the planet that was anti-correlated with precipitation and that was not apparent in the SDGVM or MPI (PC4).

The stimulation of GPP by PAR without a counteracting reduction from low precipitation in SDGVM is probably attributable to the relative insensitivity of SDGVM to low soil water avaialability when compared against other models (Medlyn *et al.*, 2016). In contrast, the ubiquity of the under-prediction in all of Earth's major agricultural regions is probably attributable

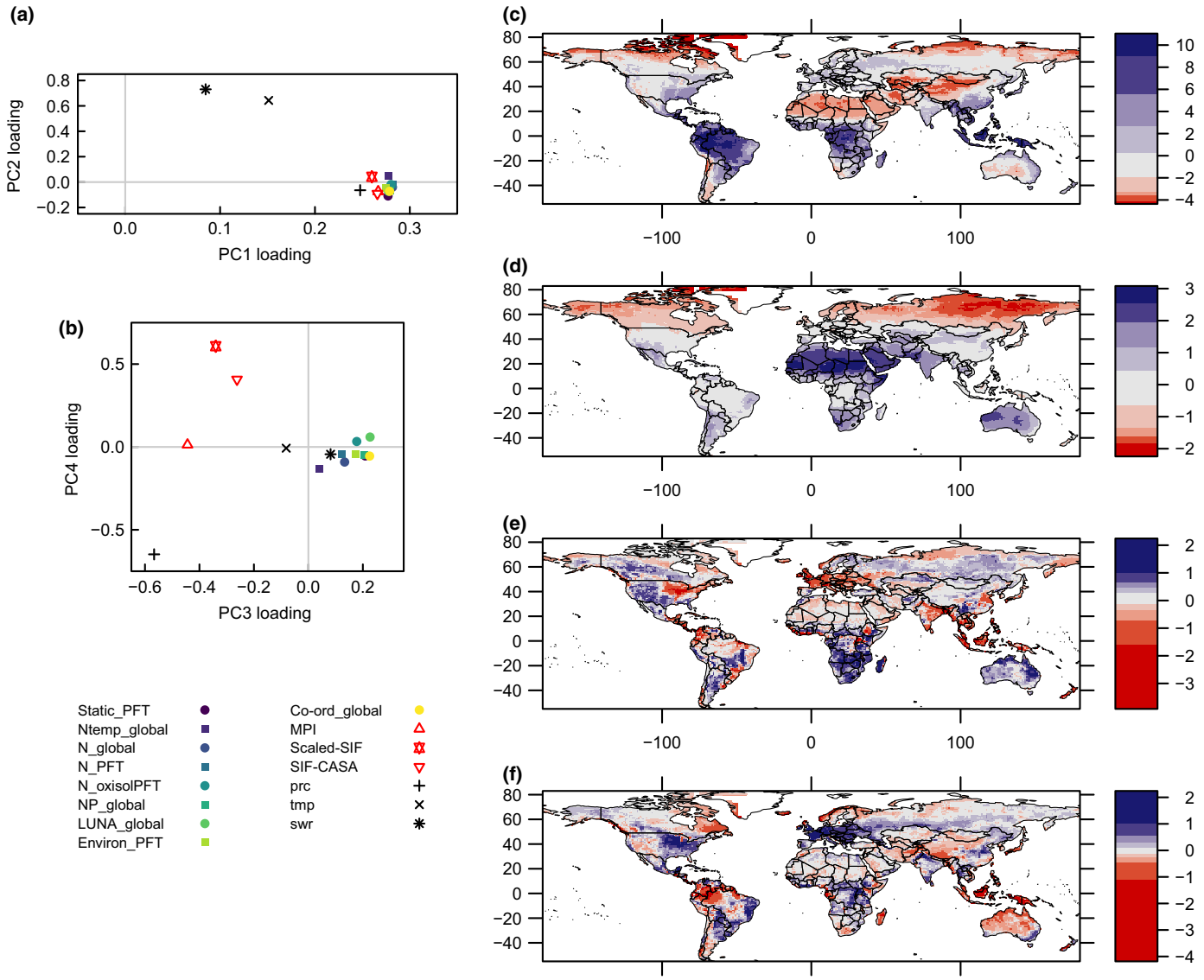

Fig. 7 Principal components (PC) analysis of the nine implementations of the four maximum photosynthetic carboxylation rate (V_{cmax}) trait-scaling hypotheses with the three gross primary production (GPP) proxies and three climatic variables: precipitation, temperature, and short-wave radiation. Loadings of variables on (a) PC1 and PC2, and (b) PC3 and PC4. Maps of (c) PC1 pattern, (d) PC2 pattern, (e) PC3 pattern, and (f) PC4 pattern. Break points on the colour scale are at quantiles (0.025, 0.1, 0.2, 0.35, 0.65, 0.8, 0.9, and 0.975) in the gridpoint scores on each PC to give even representation of the data.

to agricultural improvement which was not represented by SDGVM – for example, improved seeds, fertilization, and irrigation. The negative correlation of precipitation to PC4 and the positive SIF proxy correlation in these agricultural areas (Fig. 7) demonstrate the independence of GPP from precipitation in these regions. This independence implies that irrigation may be the primary driver of the under-prediction of GPP, while recognizing that irrigation levels are highly heterogeneous within these regions (Siebert *et al.*, 2010).

GPP proxies (MPI, SIF-CASA, and scaled-SIF) were as dissimilar to each other as the better performing hypotheses were to the proxies. PCA showed that the SIF-based proxies had higher GPP in dry, agricultural regions of the planet compared with MPI. Higher SIF-based GPP in cropland areas compared with MPI has been previously observed (Guanter *et al.*, 2014). This dissimilarity indicates an uncertain constraint from observations.

SIF is linearly related to MPI estimates of GPP at the temporal and spatial scales typically simulated by global TEMs (Guanter *et al.*, 2014; Parazoo *et al.*, 2014). SIF accurately reproduces seasonality in GPP (Joiner *et al.*, 2014), although the coefficients of the linear relationships between SIF and GPP may vary with vegetation type (Frankenberg *et al.*, 2011; Guanter *et al.*, 2012; Parazoo *et al.*, 2014). By assuming that the scaled-SIF proxy follows the same linear relationship to GPP across all terrestrial ecosystems, systematic errors (epistemic uncertainties in the classification of Beven (2016)) are likely in the scaled-SIF estimate of the global GPP distribution. However, it is also extremely likely that epistemic uncertainties are common in the system of global GPP estimation in the MPI data set – eddy-covariance flux estimates of net ecosystem exchange, empirical flux partitioning to derive GPP, derivation of empirical relationships of GPP with climate variables, and scaling of point estimated GPP using a gridded

climate data set. The scaled-SIF data are a relatively direct, global-scale signal from the photobiochemical photosynthetic pathway and their spatial distribution is entirely independent of the model output, in contrast with the MPI product and SIF-CASA, both of which use climate data in their calculation.

While the Environ_PFT had the most data-driven, and thus what we believe to be more accurate $V_{cmax,25}$ distributions, Taylor plots (Fig. 5) and difference plots (Figs 6, S7, S8) showed that its relative global GPP distributions had a larger mismatch to GPP proxies than the N limitation implementations in the northern latitudes. This difference was most apparent when compared against scaled-SIF. The latitudinal gradient in leaf N generated by the nutrient limitation implementations, and thus $V_{cmax,25}$, redistributes global GPP towards the tropics compared with other hypotheses (Figs 2, 6, S14), yielding global GPP distributions more similar to global GPP proxies.

The mismatch of the data-driven estimates of $V_{cmax,25}$ from Environ_PFT indicates latitudinal variability in the relationship of $V_{cmax,25}$ with GPP. The reason for this mismatch is unclear. SDGVM may over-predict leaf area index (LAI) in northern latitudes, and it may be that lower V_{cmax} in nutrient limitation implementations is compensating for high LAI. However, using a multi-scale state estimation procedure to combine GPP estimates from TEMs, SIF, and flux towers, Parazoo *et al.* (2014) noted a redistribution of GPP from northern latitudes to the tropics in the optimized GPP state compared with the prior estimates from the TEMs. Similar decoupling between $V_{cmax,25}$ and GPP at high latitude has also been observed in preliminary simulations of the Community Land Model (CLM version 5.0) using satellite phenology (i.e. data-driven LAI), LUNA, and observed leaf N (R. A. Fisher, pers. comm.). Alternatively, there may be insufficient V_{cmax} data for high-latuitude systems and normalizing V_{cmax} to 25°C in regions that experience these temperatures only in extreme cases and with generic temperature scaling functions could be introducing a bias in the V_{cmax} data.

Recent evidence has suggested that leaf P may modify, co-limit, or replace the $V_{cmax,25}$ to N relationship (Reich & Oleksyn, 2004; Domingues *et al.*, 2010; Walker *et al.*, 2014a; Norby *et al.*, 2017), although the physiological link to photosynthesis is more complex. Considering P limitation either implicitly (N_oxisolPFT) or explicitly (NP_global) did not clearly improve the fit to the GPP proxies (compared against their N-only counterparts) based on the quantitative comparison. However, a visual comparison of the difference plots suggests that the N_oxisolPFT implementation produced the smallest overall difference compared with GPP proxies, indicating perhaps a role for P limitation of photosynthesis in the tropics. A map of oxisols vs nonoxisols to segregate evergreen broadleaved PFTs would probably improve the simulation.

GPP trend and NBP

Most importantly for projections of the global C cycle under environmental change, the response of GPP to global change (1901–2012) across the V_{cmax} hypotheses was different, with plant-centric acclimation hypotheses showing a lower response of GPP to increasing CO_2. NBP variability over 2007–2012 was strongly related to the change in GPP over the 20th Century and the 5.4% coefficient of variation in GPP propagated through to 29% variation in NBP.

Projecting the trajectory of land C uptake is the major purpose of global terrestrial ecosystem models and the 'acclimation' of $V_{cmax,25}$ to increasing CO_2, and perhaps other factors of global change, predicted by these hypotheses has consequences for the projected terrestrial C sink. We cannot currently evaluate these consequences with data because of the difficulty in measuring GPP and terrestrial NBP, especially the 20th Century trends, although coupled Earth system models are thought to underestimate the global C sink (Hoffman *et al.*, 2014).

Co-ord_global and LUNA_global predict the shallowest, and almost indentical, GPP trends over the 20th Century (Fig. 4a). The co-ordination hypothesis (also embedded within LUNA) restricts CO_2 fertilization of GPP to the effect of CO_2 on light-limited photosynthesis. Assuming all else is equal, increasing CO_2 increases both the carboxylation-limited photosynthetic rate, w_c, and the electron transport-limited rate, w_j, but w_c is increased in greater proportion (the degree of which is dependent on the choice of model for w_j). Thus, co-ordination reduces V_{cmax} at the higher CO_2 concentration to balance w_c with w_j. Thus, under co-ordination, the CO_2 fertilization of GPP is primarily driven by the CO_2 response of light-limited photosynthesis, which is lower than the CO_2 response of carboxylation-limited photosynthesis. The decline in V_{cmax} driven by the co-ordination hypothesis is stronger than the decline in Environ_PFT (Fig. S24), which was the only hypothesis to have an explicit reduction of V_{cmax} in response to CO_2. We assumed a fixed relationship between J_{max} and V_{cmax} for the implementation of co-ordination in this analysis (Eqn 5). Given that these plant plasticity hypotheses are founded within the concept of optimality (Xu *et al.*, 2012; Prentice *et al.*, 2014; Wang *et al.*, 2014), the restriction of the CO_2 response to the smaller electron transport (light) limited response under co-ordination suggests that the optimal solution would include an increase in the J_{max} to V_{cmax} ratio as CO_2 concentrations increase.

In summary, based on an evaluation against global GPP, the analysis of multiple V_{cmax} trait scaling hypotheses suggested that nutrient limitation was the more likely driver of global V_{cmax} distributions. N limitation was implemented via a relationship of decreasing leaf N with increasing soil C based on increasing costs of N uptake. Of the nutrient limitation implementations, the PFT specific relationships to leaf N that implicitly accounted for P limitation in broadleaved evergreens (Noxisol_PFT; Kattge *et al.*, 2009) were found to most closely match the GPP proxies. Incorporating a global map of oxisols would probably help to further refine this implementation. For SDGVM and other global C cycle models, we recommend the Noxisol_PFT relationships to leaf N, particularly for models that can simulate N cycling or spatially dynamic leaf N. For carbon C only models, the Static_PFT hypothesis did not reproduce spatial distributions of global GPP as well and we suggest that the scaled relationship of N uptake to soil C (Woodward *et al.*, 1995) without the temperature modifier

could be a relatively straightforward way to implement dynamic leaf N allowing the use of the Noxisol_PFT relationships. These recommendations are contingent on the GPP proxies used, which are uncertain. We suggest that further measurements of V_{cmax} in boreal and Arctic ecosystems that include the V_{cmax} response to temperature in these ecosystems will help to discriminate among alternate hypotheses.

Acknowledgements

We thank three anonymous reviewers and the handling Editor for their time and thoughtful reviews. This material is based upon work supported by the US Department of Energy, Office of Science, Office of Biological and Environmental Research under contract number DE-AC05-00OR22725. A.P.W. and C.X. were also supported as part of the Next Generation Ecosystem Experiments-Tropics, funded by the US Department of Energy, Office of Science, Office of Biological and Environmental Research to incorporate LUNA and run final simulations. Model development by A.P.W. was supported by a PhD studentship and T.Q.'s contribution were both funded by the UK Natural Environment Research Council (NERC) National Centre for Earth Observation (NCEO). T.F.K. was supported by the Laboratory Directed Research and Development Program of Lawrence Berkeley National Laboratory under US Department of Energy Contract no. DE-AC02-05CH11231. Data and code are available on request.

Author contributions

All authors contributed to the writing of the manuscript. A.P.W. conceived of the study, ran the model, analysed the data, and led the writing. A.P.W., M.R.L., F.I.W. and T.Q. contributed to the additional developments of the SDGVM. C.X. contributed to adding the LUNA hypothesis to the SDGVM. P.M.v.B. derived the trait−environment relationships. X.Y. contributed the soil P data set. J.J. contributed SIF data. N.M. derived the land-cover data sets. M.G.D.K. and T.F.K. contributed to the analysis.

References

Ali AA, Xu C, Rogers A, Fisher RA, Wullschleger SD, Massoud EC, Vrugt JA, Muss JD, McDowell NG, Fisher JB *et al.* 2016. A global scale mechanistic model of photosynthetic capacity (LUNA V1.0). *Geoscientific Model Development* **9**: 587–606.

Ali AA, Xu C, Rogers A, McDowell NG, Medlyn BE, Fisher RA, Wullschleger SD, Reich PB, Vrugt JA, Bauerle WL *et al.* 2015. Global-scale environmental control of plant photosynthetic capacity. *Ecological Applications* **25**: 2349–2365.

Anav A, Friedlingstein P, Beer C, Ciais P, Harper A, Jones C, Murray-Tortarolo G, Papale D, Parazoo NC, Peylin P *et al.* 2015. Spatiotemporal patterns of terrestrial gross primary production: a review. *Reviews of Geophysics* **53**: 785–818.

Azevedo GFC, Marenco RA. 2012. Growth and physiological changes in saplings of *Minquartia guianensis* and *Swietenia macrophylla* during acclimation to full sunlight. *Photosynthetica* **50**: 86–94.

Beer C, Reichstein M, Tomelleri E, Ciais P, Jung M, Carvalhais N, Roedenbeck C, Arain MA, Baldocchi D, Bonan GB *et al.* 2010. Terrestrial gross carbon dioxide uptake: global distribution and covariation with climate. *Science* **329**: 834–838.

Beven K. 2016. Facets of uncertainty: epistemic uncertainty, non-stationarity, likelihood, hypothesis testing, and communication. *Hydrological Sciences Journal* **61**: 1652–1665.

van Bodegom PM, Douma JC, Verheijen LM. 2014. A fully traits-based approach to modeling global vegetation distribution. *Proceedings of the National Academy of Sciences, USA* **111**: 13733–13738.

van Bodegom PM, Douma JC, Witte JPM, Ordoñez JC, Bartholomeus RP, Aerts R. 2012. Going beyond limitations of plant functional types when predicting global ecosystem–atmosphere fluxes: exploring the merits of traits-based approaches. *Global Ecology and Biogeography* **21**: 625–636.

Bonan GB, Lawrence PJ, Oleson KW, Levis S, Jung M, Reichstein M, Lawrence DM, Swenson SC. 2011. Improving canopy processes in the Community Land Model version 4 (CLM4) using global flux fields empirically inferred from FLUXNET data. *Journal of Geophysical Research: Biogeosciences* **116**: G02014.

Brzostek ER, Fisher JB, Phillips RP. 2014. Modeling the carbon cost of plant nitrogen acquisition: mycorrhizal trade-offs and multipath resistance uptake improve predictions of retranslocation. *Journal of Geophysical Research: Biogeosciences* **119**: 1684–1697.

von Caemmerer S. 2000. *Biochemical models of leaf photosynthesis*. Collingwood, Victoria, Australia: CSIRO Publishing.

Cernusak LA, Hutley LB, Beringer J, Holtum JAM, Turner BL. 2011. Photosynthetic physiology of eucalypts along a sub-continental rainfall gradient in northern Australia. *Agricultural and Forest Meteorology* **151**: 1462–1470.

Chen JL, Reynolds JF, Harley PC, Tenhunen JD. 1993. Coordination theory of leaf nitrogen distribution in a canopy. *Oecologia* **93**: 63–69.

Craine JM, Tilman D, Wedin D, Reich P, Tjoelker M, Knops J. 2002. Functional traits, productivity and effects on nitrogen cycling of 33 grassland species. *Functional Ecology* **16**: 563–574.

Cramer W, Bondeau A, Woodward FI, Prentice IC, Betts RA, Brovkin V, Cox PM, Fisher V, Foley JA, Friend AD *et al.* 2001. Global response of terrestrial ecosystem structure and function to CO_2 and climate change: results from six dynamic global vegetation models. *Global Change Biology* **7**: 357–373.

De Kauwe MG, Medlyn BE, Zaehle S, Walker AP, Dietze MC, Hickler T, Jain AK, Luo Y, Parton WJ, Prentice IC *et al.* 2013. Forest water use and water use efficiency at elevated CO_2: a model-data intercomparison at two contrasting temperate forest FACE sites. *Global Change Biology* **19**: 1759–1779.

De Kauwe MG, Medlyn BE, Zaehle S, Walker AP, Dietze MC, Wang Y-P, Luo Y, Jain AK, El-Masri B, Hickler T *et al.* 2014. Where does the carbon go? A model–data intercomparison of vegetation carbon allocation and turnover processes at two temperate forest free-air CO_2 enrichment sites. *New Phytologist* **203**: 883–899.

Deng X, Ye WH, Feng HL, Yang QH, Cao HL, Hui KY, Zhang Y. 2004. Gas exchange characteristics of the invasive species *Mikania micrantha* and its indigenous congener *M. cordata* (Asteraceae) in South China. *Botanical Bulletin of Academia Sinica* **45**: 213–220.

Domingues TF, Ishida FY, Feldpausch TR, Grace J, Meir P, Saiz G, Sene O, Schrodt F, Sonké B, Taedoumg H *et al.* 2015. Biome-specific effects of nitrogen and phosphorus on the photosynthetic characteristics of trees at a forest-savanna boundary in Cameroon. *Oecologia* **178**: 659–672.

Domingues TF, Meir P, Feldpausch TR, Saiz G, Veenendaal EM, Schrodt F, Bird M, Djagbletey G, Hien F, Compaore H *et al.* 2010. Co-limitation of photosynthetic capacity by nitrogen and phosphorus in West Africa woodlands. *Plant, Cell & Environment* **33**: 959–980.

Farquhar GD, von Caemmerer S, Berry JA. 1980. A biochemical model of photosynthetic CO_2 assimilation in leaves of C_3 species. *Planta* **149**: 78–90.

Field CB, Mooney HA. 1986. The leaf nitrogen-photosynthesis relationship. In: Givnish TJ, ed. *On the economy of plant form and function*. Cambridge, UK: Cambridge University Press, 25–55.

Fisher JB, Sitch S, Malhi Y, Fisher RA, Huntingford C, Tan S-Y. 2010. Carbon cost of plant nitrogen acquisition: a mechanistic, globally applicable model of plant nitrogen uptake, retranslocation, and fixation. *Global Biogeochemical Cycles* **24**: GB1014.

Fisher RA, Muszala S, Verteinstein M, Lawrence P, Xu C, McDowell NG, Knox RG, Koven C, Holm J, Rogers BM *et al.* 2015. Taking off the training wheels: the properties of a dynamic vegetation model without climate envelopes, CLM4.5(ED). *Geoscientific Model Development* **8**: 3593–3619.

Frankenberg C, Fisher JB, Worden J, Badgley G, Saatchi SS, Lee J-E, Toon GC, Butz A, Jung M, Kuze A *et al.* 2011. New global observations of the terrestrial carbon cycle from GOSAT: patterns of plant fluorescence with gross primary productivity. *Geophysical Research Letters* **38**: L17706.

Friend AD, Lucht W, Rademacher TT, Keribin R, Betts R, Cadule P, Ciais P, Clark DB, Dankers R, Falloon PD *et al.* 2014. Carbon residence time dominates uncertainty in terrestrial vegetation responses to future climate and atmospheric CO_2. *Proceedings of the National Academy of Sciences, USA* **111**: 3280–3285.

Fyllas NM, Gloor E, Mercado LM, Sitch S, Quesada CA, Domingues TF, Galbraith DR, Torre-Lezama A, Vilanova E, Ramírez-Angulo H *et al.* 2014. Analysing Amazonian forest productivity using a new individual and trait-based model (TFS v. 1). *Geoscientific Model Development* **7**: 1251–1269.

Grime JP. 1974. Vegetation classification by reference to strategies. *Nature* **250**: 26–31.

Guanter L, Frankenberg C, Dudhia A, Lewis PE, Gómez-Dans J, Kuze A, Suto H, Grainger RG. 2012. Retrieval and global assessment of terrestrial chlorophyll fluorescence from GOSAT space measurements. *Remote Sensing of Environment* **121**: 236–251.

Guanter L, Zhang Y, Jung M, Joiner J, Voigt M, Berry JA, Frankenberg C, Huete AR, Zarco-Tejada P, Lee J-E *et al.* 2014. Global and time-resolved monitoring of crop photosynthesis with chlorophyll fluorescence. *Proceedings of the National Academy of Sciences, USA* **111**: E1327–E1333.

Harley PC, Thomas RB, Reynolds JF, Strain BR. 1992. Modeling photosynthesis of cotton grown in elevated CO_2. *Plant, Cell & Environment* **15**: 271–282.

Hoffman FM, Randerson JT, Arora VK, Bao Q, Cadule P, Ji D, Jones CD, Kawamiya M, Khatiwala S, Lindsay K *et al.* 2014. Causes and implications of persistent atmospheric carbon dioxide biases in Earth System Models. *Journal of Geophysical Research: Biogeosciences* **119**: 141–162.

Joiner J, Guanter L, Lindstrot R, Voigt M, Vasilkov AP, Middleton EM, Huemmrich KF, Yoshida Y, Frankenberg C. 2013. Global monitoring of terrestrial chlorophyll fluorescence from moderate-spectral-resolution near-infrared satellite measurements: methodology, simulations, and application to GOME-2. *Atmospheric Measurement Techniques* **6**: 2803–2823.

Joiner J, Yoshida Y, Guanter L, Middleton EM. 2016. New methods for the retrieval of chlorophyll red fluorescence from hyperspectral satellite instruments: simulations and application to GOME-2 and SCIAMACHY. *Atmospheric Measurement Techniques* **9**: 3939–3967.

Joiner J, Yoshida Y, Vasilkov AP, Schaefer K, Jung M, Guanter L, Zhang Y, Garrity S, Middleton EM, Huemmrich KF *et al.* 2014. The seasonal cycle of satellite chlorophyll fluorescence observations and its relationship to vegetation phenology and ecosystem atmosphere carbon exchange. *Remote Sensing of Environment* **152**: 375–391.

Jung M, Reichstein M, Margolis HA, Cescatti A, Richardson AD, Arain MA, Arneth A, Bernhofer C, Bonal D, Chen J *et al.* 2011. Global patterns of land-atmosphere fluxes of carbon dioxide, latent heat, and sensible heat derived from eddy covariance, satellite, and meteorological observations. *Journal of Geophysical Research: Biogeosciences* **116**: G00J07.

Kattge J, Diaz S, Lavorel S, Prentice C, Leadley P, Boenisch G, Garnier E, Westoby M, Reich PB, Wright IJ *et al.* 2011. TRY – a global database of plant traits. *Global Change Biology* **17**: 2905–2935.

Kattge J, Knorr W. 2007. Temperature acclimation in a biochemical model of photosynthesis: a reanalysis of data from 36 species. *Plant, Cell & Environment* **30**: 1176–1190.

Kattge J, Knorr W, Raddatz T, Wirth C. 2009. Quantifying photosynthetic capacity and its relationship to leaf nitrogen content for global-scale terrestrial biosphere models. *Global Change Biology* **15**: 976–991.

Keeling CD, Piper SC, Bacastow RB, Wahlen M, Whorf TP, Heimann M, Meijer HA. 2005. Atmospheric CO_2 and $^{13}CO_2$ exchange with the terrestrial biosphere and oceans from 1978 to 2000: observations and carbon cycle implications. In: Ehlringer JR, Cerling TE, Dearing MD, eds. *A history of atmospheric CO_2 and its effects on plants, animals, and ecosystems*. New York, NY, USA: Springer, 83–113.

Kueppers L, Iversen C, Koven C. 2016. Expanding use of plant trait observation in earth system models. *Eos* **97**: https://doi.org/10.1029/2016eo049947.

Kumar J, Hoffman FM, Hargrove WW, Collier N. 2016. Understanding the representativeness of FLUXNET for upscaling carbon flux from eddy covariance measurements. *Earth System Science Data Discussions*. https://doi.org/10.5194/essd-2016-36.

Le Quéré C, Peters GP, Andres RJ, Andrew RM, Boden TA, Ciais P, Friedlingstein P, Houghton RA, Marland G, Moriarty R *et al.* 2014. Global carbon budget 2013. *Earth System Science Data* **6**: 235–263.

Lemon J. 2006. Plotrix: a package in the red light district of R. *R-News* **6**: 8–12.

Maire V, Martre P, Kattge J, Gastal F, Esser G, Fontaine S, Soussana J-F. 2012. The coordination of leaf photosynthesis links C and N fluxes in C_3 plant species. *PLoS ONE* **7**: e38345.

McGroddy ME, Daufresne T, Hedin LO. 2004. Scaling of C : N : P stoichiometry in forests worldwide: implications of terrestrial redfield-type ratios. *Ecology* **85**: 2390–2401.

Medlyn BE, De Kauwe MG, Zaehle S, Walker AP, Duursma RA, Luus K, Mishurov M, Pak B, Smith B, Wang Y-P *et al.* 2016. Using models to guide field experiments: *a priori* predictions for the CO_2 response of a nutrient- and water-limited native Eucalypt woodland. *Global Change Biology* **22**: 2834–2851.

Medlyn BE, Dreyer E, Ellsworth D, Forstreuter M, Harley PC, Kirschbaum MUF, Le Roux X, Montpied P, Strassemeyer J, Walcroft A *et al.* 2002. Temperature response of parameters of a biochemically based model of photosynthesis. II. A review of experimental data. *Plant, Cell & Environment* **25**: 1167–1179.

Medlyn BE, Zaehle S, De Kauwe MG, Walker AP, Dietze MC, Hanson PJ, Hickler T, Jain AK, Luo Y, Parton W *et al.* 2015. Using ecosystem experiments to improve vegetation models. *Nature Climate Change* **5**: 528–534.

Meir P, Levy PE, Grace J, Jarvis PG. 2007. Photosynthetic parameters from two contrasting woody vegetation types in West Africa. *Plant Ecology* **192**: 277–287.

Nascimento HCS, Marenco RA. 2013. Mesophyll conductance variations in response to diurnal environmental factors in *Myrcia paivae* and *Minquartia guianensis* in Central Amazonia. *Photosynthetica* **51**: 457–464.

Niinemets Ü. 1999. Components of leaf dry mass per area – thickness and density – alter leaf photosynthetic capacity in reverse directions in woody plants. *New Phytologist* **144**: 35–47.

Norby RJ, Gu L, Haworth IC, Jensen AM, Turner BL, Walker AP, Warren JM, Weston DJ, Xu C, Winter K. 2017. Informing models through empirical relationships between foliar phosphorus, nitrogen and photosynthesis across diverse woody species in tropical forests of Panama. *New Phytologist* **215**: 1425–1437.

Ordonez JC, van Bodegom PM, Witte J-PM, Wright IJ, Reich PB, Aerts R. 2009. A global study of relationships between leaf traits, climate and soil measures of nutrient fertility. *Global Ecology and Biogeography* **18**: 137–149.

Parazoo NC, Bowman K, Fisher JB, Frankenberg C, Jones DBA, Cescatti A, Pérez-Priego Ó, Wohlfahrt G, Montagnani L. 2014. Terrestrial gross primary production inferred from satellite fluorescence and vegetation models. *Global Change Biology* **20**: 3103–3121.

Pavlick R, Drewry DT, Bohn K, Reu B, Kleidon A. 2013. The Jena Diversity-Dynamic Global Vegetation Model (JeDi-DGVM): a diverse approach to representing terrestrial biogeography and biogeochemistry based on plant functional trade-offs. *Biogeosciences* **10**: 4137–4177.

Picard G, Woodward FI, Lomas MR, Pellenq J, Quegan S, Kennedy M. 2005. Constraining the Sheffield dynamic global vegetation model using stream-flow measurements in the United Kingdom. *Global Change Biology* **11**: 2196–2210.

Poulter B, MacBean N, Hartley A, Khlystova I, Arino O, Betts R, Bontemps S, Boettcher M, Brockmann C, Defourny P *et al.* 2015. Plant functional type classification for earth system models: results from the European Space Agency's Land Cover Climate Change Initiative. *Geoscientific Model Development* **8**: 2315–2328.

Prentice IC, Dong N, Gleason SM, Maire V, Wright IJ. 2014. Balancing the costs of carbon gain and water transport: testing a new theoretical framework for plant functional ecology. *Ecology Letters* **17**: 82–91.

R Core Development Team. 2011. *R: a language and environment for statistical computing*. Vienna, Austria: R Foundation for Statistical Computing.

Read DJ. 1991. Mycorrhizas in ecosystems. *Experientia* **47**: 376–391.

Reich PB. 2014. The world-wide 'fast–slow' plant economics spectrum: a traits manifesto. *Journal of Ecology* **102**: 275–301.

Reich PB, Oleksyn J. 2004. Global patterns of plant leaf N and P in relation to temperature and latitude. *Proceedings of the National Academy of Sciences, USA* **101**: 11001–11006.

Rogers A. 2014. The use and misuse of $V_{c,max}$ in Earth System Models. *Photosynthesis Research* **119**: 15–29.

Rogers A, Medlyn BE, Dukes JS, Bonan G, von Caemmerer S, Dietze MC, Kattge J, Leakey ADB, Mercado LM, Niinemets Ü *et al.* 2017. A roadmap for improving the representation of photosynthesis in Earth system models. *New Phytologist* **213**: 22–42.

Sargsyan K, Safta C, Najm HN, Debusschere BJ, Ricciuto D, Thornton P. 2014. Dimensionality reduction for complex models via bayesian compressive sensing. *International Journal for Uncertainty Quantification* **4**: 63–93.

Scheiter S, Langan L, Higgins SI. 2013. Next-generation dynamic global vegetation models: learning from community ecology. *New Phytologist* **198**: 957–969.

Siebert S, Burke J, Faures JM, Frenken K, Hoogeveen J, Döll P, Portmann FT. 2010. Groundwater use for irrigation – a global inventory. *Hydrology and Earth System Sciences* **14**: 1863–1880.

Sitch S, Huntingford C, Gedney N, Levy PE, Lomas M, Piao SL, Betts R, Ciais P, Cox P, Friedlingstein P *et al.* 2008. Evaluation of the terrestrial carbon cycle, future plant geography and climate-carbon cycle feedbacks using five Dynamic Global Vegetation Models (DGVMs). *Global Change Biology* **14**: 2015–2039.

Smith TM, Shugart HH, Woodward FI, Eds. 1998. *Plant functional types: their relevance to ecosystem properties and global change*. Cambridge, UK: Cambridge University Press.

Taylor KE. 2001. Summarizing multiple aspects of model performance in a single diagram. *Journal of Geophysical Research: Atmospheres* **106**: 7183–7192.

Vårhammar A, Wallin G, McLean CM, Dusenge ME, Medlyn BE, Hasper TB, Nsabimana D, Uddling J. 2015. Photosynthetic temperature responses of tree species in Rwanda: evidence of pronounced negative effects of high temperature in montane rainforest climax species. *New Phytologist* **206**: 1000–1012.

Verheijen LM, Aerts R, Brovkin V, Cavender-Bares J, Cornelissen JHC, Kattge J, van Bodegom PM. 2015. Inclusion of ecologically based trait variation in plant functional types reduces the projected land carbon sink in an earth system model. *Global Change Biology* **21**: 3074–3086.

Verheijen LM, Brovkin V, Aerts R, Bönisch G, Cornelissen JHC, Kattge J, Reich PB, Wright IJ, van Bodegom PM. 2013. Impacts of trait variation through observed trait–climate relationships on performance of an Earth system model: a conceptual analysis. *Biogeosciences* **10**: 5497–5515.

Walker AP, Beckerman AP, Gu L, Kattge J, Cernusak LA, Domingues TF, Scales JC, Wohlfahrt G, Wullschleger SD, Woodward FI. 2014a. The relationship of leaf photosynthetic traits – V_{cmax} and J_{max} – to leaf nitrogen, leaf phosphorus, and specific leaf area: a meta-analysis and modeling study. *Ecology and Evolution* **4**: 3218–3235.

Walker AP, Hanson PJ, De Kauwe MG, Medlyn BE, Zaehle S, Asao S, Dietze M, Hickler T, Huntingford C, Iversen CM *et al.* 2014b. Comprehensive ecosystem model-data synthesis using multiple data sets at two temperate forest free-air CO_2 enrichment experiments: model performance at ambient CO_2 concentration. *Journal of Geophysical Research: Biogeosciences* **119**: 937–964.

Wang H, Prentice IC, Davis TW. 2014. Biophsyical constraints on gross primary production by the terrestrial biosphere. *Biogeosciences* **11**: 5987–6001.

van de Weg MJ, Meir P, Grace J, Ramos GD. 2011. Photosynthetic parameters, dark respiration and leaf traits in the canopy of a Peruvian tropical montane cloud forest. *Oecologia* **168**: 23–34.

van der Werf GR, Randerson JT, Giglio L, Collatz GJ, Mu M, Kasibhatla PS, Morton DC, DeFries RS, Jin Y, van Leeuwen TT. 2010. Global fire emissions and the contribution of deforestation, savanna, forest, agricultural, and peat fires (1997–2009). *Atmospheric Chemistry and Physics* **10**: 11707–11735.

Woodward FI, Cramer W. 1996. Plant functional types and climatic change: introduction. *Journal of Vegetation Science* **7**: 306–308.

Woodward FI, Lomas MR. 2004. Vegetation dynamics – simulating responses to climatic change. *Biological Reviews* **79**: 643–670.

Woodward FI, Smith TM. 1994. Global photosynthesis and stomatal conductance – modeling the controls by soil and climate. In: Callow JA, ed. *Advances in Botanical Research* **20**: 1–41.

Woodward FI, Smith TM. 1995. Predictions and measurements of the maximum photosynthetic rate, A_{max}, at the global scale. In: Schulze E-D, Caldwell MM, eds. *Springer Study Edition. Ecophysiology of photosynthesis*. Berlin, Heidelberg, Germany: Springer, 491–509.

Woodward FI, Smith TM, Emanuel WR. 1995. A global land primary productivity and phytogeography model. *Global Biogeochemical Cycles* **9**: 471–490.

Wright IJ, Reich PB, Westoby M, Ackerly DD, Baruch Z, Bongers F, Cavender-Bares J, Chapin T, Cornelissen JHC, Diemer M *et al.* 2004. The worldwide leaf economics spectrum. *Nature* **428**: 821–827.

Wullschleger SD, Epstein HE, Box EO, Euskirchen ES, Goswami S, Iversen CM, Kattge J, Norby RJ, van Bodegom PM, Xu X. 2014. Plant functional types in Earth system models: past experiences and future directions for application of dynamic vegetation models in high-latitude ecosystems. *Annals of Botany* **114**: 1–16.

Xu C, Fisher R, Wullschleger SD, Wilson CJ, Cai M, McDowell NG. 2012. Toward a mechanistic modeling of nitrogen limitation on vegetation dynamics. *PLoS ONE* **7**: e37914.

Yang X, Post WM, Thornton PE, Jain AK. 2014. *Global gridded soil phosphorus distribution maps at 0.5-degree resolution*. Oak Ridge, TN, USA: ORNL DAAC.

Zaehle S, Medlyn BE, De Kauwe MG, Walker AP, Dietze MC, Hickler T, Luo Y, Wang Y-P, El-Masri B, Thornton P *et al.* 2014. Evaluation of 11 terrestrial carbon–nitrogen cycle models against observations from two temperate Free-Air CO_2 Enrichment studies. *New Phytologist* **202**: 803–822.

Zaehle S, Sitch S, Smith B, Hatterman F. 2005. Effects of parameter uncertainties on the modeling of terrestrial biosphere dynamics. *Global Biogeochemical Cycles* **19**: GB3020.

Supporting Information

Additional Supporting Information may be found online in the Supporting Information tab for this article:

Fig. S1 Temperature responses of V_{cmax}.

Figs S2–S4 Climate data used to run the model.

Figs S5–S12 Land-cover data used to run the model.

Fig. S13 Zonal plot of $V_{cmax,25}$.

Fig. S14 Zonal plot of GPP.

Fig. S15 Global GPP for various V_{cmax} temperature scaling assumptions.

Fig. S16 20th and 21st change in GPP for various V_{cmax} temperature scaling assumptions.

Fig. S17 GPP observation proxies.

Fig. S18 Difference plot of model GPP to MPI GPP proxy.

Fig. S19 Difference plot of model GPP to SIF-CASA GPP proxy.

Fig. S20 Variance explained by each principal component.

Figs S21–S23 Modelled relationships between leaf N and $V_{cmax,25}$ with soil carbon.

Fig. S24 20th and 21st change in modelled $V_{cmax,25}$.

Table S1 Metrics for Taylor plots

Notes S1 Additional methods description.

Please note: Wiley Blackwell are not responsible for the content or functionality of any Supporting Information supplied by the authors. Any queries (other than missing material) should be directed to the *New Phytologist* Central Office.